An Improved Algorithm for Estimating the Secchi Disk Depth from Remote Sensing Data Based on the New Underwater Visibility Theory

Dalin Jiang[1], Bunkei Matsushita[2*], Setiawan Fajar[1], Augusto Vundo[1]

[1]Graduate School of Life and Environmental Sciences, University of Tsukuba, Tsukuba, Ibaraki, 305-8572, Japan

[2]Faculty of Life and Environmental Sciences, University of Tsukuba, Tsukuba, Ibaraki, 305-8572, Japan

Submittal date: April 1, 2019

*Corresponding Author

Phone: 81-29-853-7190

Fax: 81-29-853-7190

Email: matsushita.bunkei.gn@u.tsukuba.ac.jp

An Improved Algorithm for Estimating the Secchi Disk Depth from Remote Sensing Data Based on the New Underwater Visibility Theory

Abstract

The Secchi disk depth (Z_{SD}) is a widely used parameter for evaluating water clarity. Here we propose an improved algorithm, which is based on a new underwater visibility theory, for retrieving more accurate Z_{SD} from remote sensing reflectance (R_{rs}) in various waters. Two improvements were carried out in the new algorithm. First, we used a hybrid quasi-analytical algorithm (QAA_hybrid) instead of the sixth version of QAA (QAA_v6) for retrieving more accurate total absorption coefficient ($a(\lambda)$) and total backscattering coefficient ($b_b(\lambda)$) even in turbid inland waters. Second, we used a dynamic K_T/K_d ratio (i.e., ratio of diffuse attenuation coefficient of upwelling radiance and diffuse attenuation coefficient of downwelling irradiance) instead of using the fixed ratio (i.e., 1.5). The results obtained from in situ R_{rs} show that the improved Z_{SD} estimation algorithm gave more accurate Z_{SD} estimations, with the root mean square error (RMSE) reduced from 0.2 to 0.1 in log10 unit, mean absolute percentage error (MAPE) reduced from 39 % to 20 % (N=178 with in situ Z_{SD} values between 0.3 – 20.8 m). We then applied the improved Z_{SD} estimation algorithm to the 2003–2012 MERIS images for Lake Kasumigaura to further confirm the performance of the improved Z_{SD} estimation algorithm. The results obtained from 19 matchups demonstrate that the estimated Z_{SD} matched well with the in situ Z_{SD}, with the RMSE of 0.11 m and the MAPE of 15%. The improved Z_{SD} estimation algorithm shows a potential to estimate more accurate Z_{SD} values from remote sensing data in various waters.

Keywords: Secchi disk depth, quasi-analytical algorithm, remote sensing, various waters, hybrid

1. Introduction

The Secchi disk depth (Z_{SD}), also termed 'water clarity' or 'transparency' in aquatic sciences, is a direct record of water optics and an important indicator of water quality (Wernand et al., 2010). Therefore, the Z_{SD} has been a routine measurement in field survey of aquatic environments using a called Secchi disk since the 1860s (Secchi, 1864). Over a century later, the remote sensing technique has also been widely used for retrieving the Z_{SD} values because of the technique's large area coverage and rapid data acquisition (Yarger and McCauley, 1975; Carlson, 1977). Generally, there are two approaches for retrieving the Z_{SD} from remote sensing data: empirical and semi-analytical approaches. The empirical approach usually estimates the Z_{SD} by directly carrying out a regression analysis between the remote sensing data and in situ Z_{SD} measurements (e.g., Giardino et al., 2001; Kloiber et al., 2002; Kratzer et al., 2003; Chen et al., 2007; Olmanson et al., 2008; Kabbara et al., 2008; Kratzer et al., 2008; Zhao et al., 2011; Olmanson et al., 2016).

In contrast, the semi-analytical approach retrieves the Z_{SD} based on an underwater visibility theory (Doron et al., 2011; Fukushima et al., 2016, 2018; Alikas and Kratzer, 2017; Rodrigues et al., 2017). Compared to the empirical approach, the semi-analytical approach has two advantages: (1) a clearer mechanism and thus more reliable results; and (2) this approach often does not need in situ data for recalibrating the retrieval algorithm. It can thus be considered that the semi-analytical approach would be more useful for monitoring the Z_{SD} in various water bodies, especially for those that lack in situ measurements.

Before 2015, semi-analytical algorithms for Z_{SD} retrieval were based mainly on an underwater visibility theory proposed by Duntley (1952) (hereafter referred to as the 'classical theory'). According to the classical theory, the Z_{SD} is inversely proportional to the sum of the beam attenuation coefficient (c, m^{-1}) and the diffuse attenuation coefficient of downwelling irradiance (K_d, m^{-1}) within the visible domain (Tyler, 1968; Preisendorfer, 1986). However, Lee et al. (2015a, 2018) pointed out that there are some drawbacks or mistakes in the classical theory, which has been used for more than 60 years. First, the critical assumption, i.e., that the radiance distribution over the target is equal to the radiance distribution over the background, may not be valid for water bodies because a 30-cm Secchi disk cannot be treated as a point at a distance shorter than tens of meters. Second, the use of full visible domain to determine a Z_{SD} value is not appropriate because how far the human eye-brain system is able to see should depend on information from a visible wavelength with maximum transmittance in a water body. Third, the use of relative difference between water and Secchi disk just match the sharpness of an object, which is not the case of using a 30-cm Secchi disk to measure Z_{SD} within tens of meters.

To overcome the above problems, Lee et al. (2015a) proposed a new theory for underwater visibility (hereafter referred to as the 'new theory'). Based on this new theory, Lee et al. also developed a semi-analytical algorithm for retrieving the Z_{SD} from remote sensing data (hereafter referred to as the 'Lee15'). The Lee15 algorithm is comprised of three main steps: (1) retrieving the total absorption coefficient $a(\lambda)$ and the total backscattering coefficient $b_b(\lambda)$ from the remote sensing reflectance $R_{rs}(\lambda)$ by using the sixth version of the quasi-analytical algorithm (QAA_v6, Lee et al., 2002; IOCCG, 2014); (2) calculating the $K_d(\lambda)$ from $a(\lambda)$ and $b_b(\lambda)$ as well as the corresponding solar zenith angle by using a semi-analytical model developed by Lee et al. (2005, 2013); and (3) estimating the Z_{SD} from the selected minimum K_d and the corresponding R_{rs} at the visible bands.

However, several research groups have reported that the QAA_v6 or its previous version (QAA_v5) often failed in turbid inland waters (Le et al., 2009; Yang et al., 2013; Huang et al., 2014; Mishra et al., 2014; Watanabe et al., 2016; Wang et al., 2017). It can be speculated that the estimation errors of $a(\lambda)$ and $b_b(\lambda)$ will be propagated to the estimations of $K_d(\lambda)$ and then the final estimations of the Z_{SD}. Some of the above-cited groups also sought to modify the QAA_v6 or QAA_v5 for obtaining more accurate $a(\lambda)$ and $b_b(\lambda)$ values in turbid inland waters. It is thus necessary to integrate these new endeavors into the Lee15 algorithm to improve its applicability for various water bodies around the world.

Another potential error source in the Lee15 algorithm is the assumption of a constant ratio of the upwelling radiance diffuse attenuation coefficient (K_T) and K_d. Empirically, the ratio value of 1.5 was used in the Lee15 algorithm (i.e., $K_T = 1.5K_d$). However, a wide range of ratios have been reported (0.5–2.0). For example, Philpot (1989) pointed out that the reasonable range for K_T/K_d was from 0.5 to 2. Maritorena et al. (1994) reported that K_T/K_d ranged from 1.02 to 1.66 based on simulations. A K_T/K_d range of 1.4–1.7 can also be estimated when the solar zenith angle $\theta = 0$ degrees according to Lee et al. (1994). It can thus be speculated that using a fixed K_T/K_d value in a Z_{SD} estimation may lead to errors, and more realistic K_T/K_d ratios are needed to further improve the performance of the Lee15 algorithm.

We therefore conducted the present study to: (1) improve the Lee15 algorithm for estimating the Z_{SD} values in various waters by integrating different types of QAAs and dynamic K_T/K_d ratios into the original algorithm, and (2) evaluate the performance of the improved Lee15 algorithm using in situ data collected from several Japanese lakes and SeaBASS dataset as well as MERIS (MEdium Resolution Imaging Spectrometer) data over Lake Kasumigaura, Japan.

2. Study Area and Data Collection

2.1. Study area

The study area of this research included 8 lakes in Japan (Fig. 1a) and coastal waters in United States. The 8 Japanese lakes include Lakes Biwa, Kasumigaura, Akan, Suwa, Motosu, Sai, Unagi, and Shirakaba. The water quality parameters of these lakes varied widely, with Z_{SD} values from 0.4 m to 16.4 m, chlorophyll-a concentrations ranging from 0.5 mg/m^3 to 148.6 mg/m^3, and total suspended solids (TSS) ranging from 0.4 g/m^3 to 45.6 g/m^3 (Table 1). The coastal waters in United States include San Francisco Bay and the northern Gulf of Mexico (Fig.1c). In total 129 in situ-measured R_{rs} spectra with corresponding Z_{SD} were collected from the SeaBASS dataset, and the Z_{SD} values ranged from 0.3 m to 20.8 m.

Lake Kasumigaura, with a surface area of 220 km^2 and a mean water depth of 4 m, was also used for MERIS data analyses (Fig. 1b). Its Z_{SD} values ranged from 0.4 m to 1.2 m. The chlorophyll-a concentration ranged from 12.0 mg/m^3 to 148.6 mg/m^3 and the TSS ranged from 4.1 g/m^3 to 45.6 g/m^3 in this lake. There are 10 routine monitoring sites in Lake Kasumigaura with a monitoring frequency of 1 month.

Table 1. Area, depth, water quality, and number of collected data of 8 Japanese studied lakes

Lake name	Area (km^2)	Maximum depth (m)	Z_{SD} (m)	Chl-a (mg/m^3)	TSS (g/m^3)	Number of data
Biwa	670.3	103.8	3.2-9.3	0.7-2.9	0.6-2.0	15
Kasumigaura	220.0	11.9	0.4-1.2	12.0-148.6	4.1-45.6	77
Akan	13.0	44.8	6.7	0.8	1.5	1
Suwa	12.9	7.6	0.9-1.9	9.8-29.4	4.6-9.6	16
Motosu	4.7	121.6	16.4	0.6	0.4	1
Sai	2.1	71.7	6.8-7.1	1.8	1.3	2
Unagi	1.2	55.8	12.8	0.5	0.4	1
Shirakaba	0.4	9.1	3.5	2.3	2.8	1

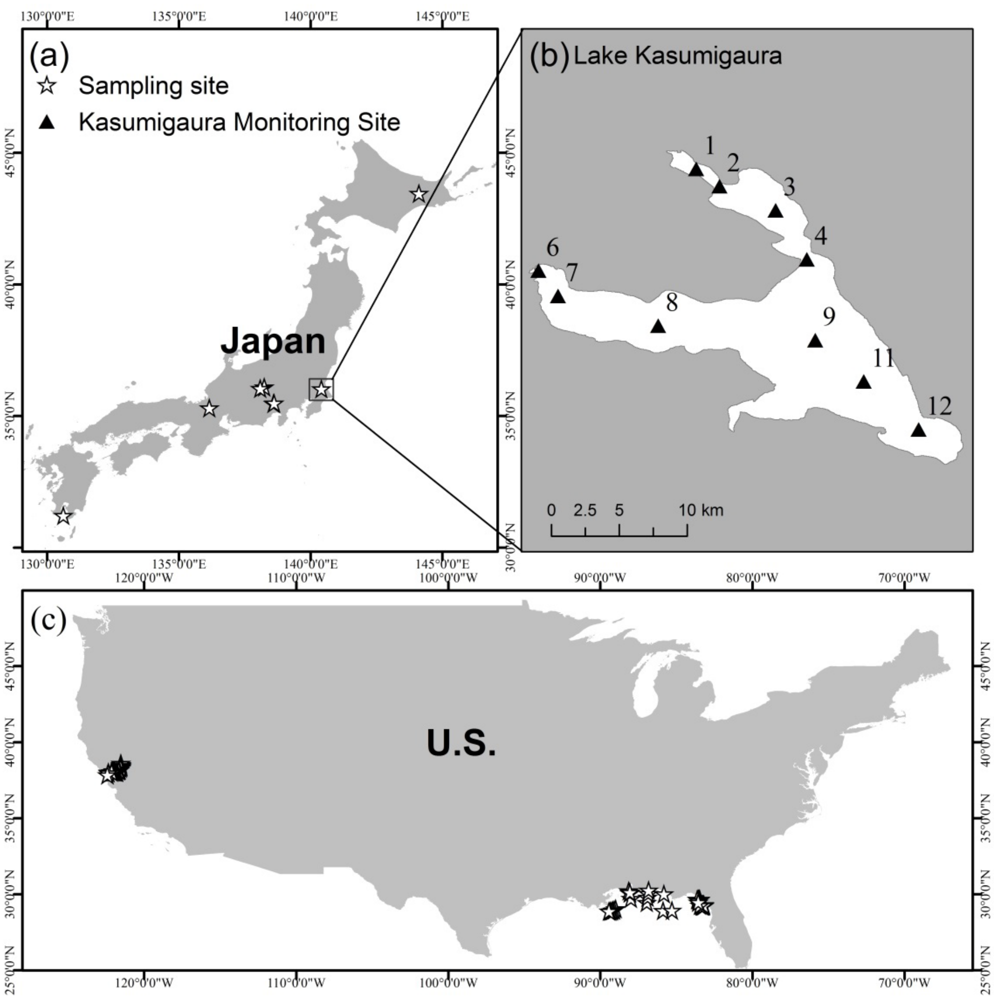

Fig. 1. Study area. (a) Field samplings were carried out in 8 lakes in Japan. (b) Lake Kasumigaura (only western part is shown) and its 10 routine monitoring sites. (c) Sampling sites of data collected from SeaBASS.

2.2. In situ data collection and processing

Field surveys were carried out in the 8 above-described Japanese lakes during 2009–2016. Data were collected from a total of 114 sampling sites. For each site, the Z_{SD} was measured by vertically lowering down a 30-cm-dia. white disk into the water until the disk was no longer visible (or lower a Secchi disk out of sight and then raise the disk until it becomes visible). At the same time, the radiance of skylight (L_s), the radiance from a standard gray board (L_g), and the total upwelling radiance from the water (L_t) were measured using a FieldSpec® HandHeld spectroradiometer (ASD Inc., Bloulder, CO, USA) between the local time 9:30 to 14:00 (three measurements between 14:00 and 16:00), with the sensor zenith angle of 40° and azimuth angle of 135° from the sun.

Remote sensing reflectance (R_{rs}) was then calculated using the following equation:

$$R_{rs} = (L_t - \rho L_s) / \left(\frac{\pi}{R_g} L_g \right) - \Delta \qquad (1)$$

where ρ is the skylight reflectance (0.028 when the wind speed was <5 m/sec, Mobley, 1999), and R_g is the reflectance of the gray board; Δ is the contribution of the residual reflected skylight, which was calculated from the median R_{rs} value between the wavelengths of 950 and 1000 nm for turbid water and 800–850 nm for clear water. This is because the absorption coefficient of pure water is extremely high (it can reach 48 m^{-1}) at the wavelengths of 950–1000 nm (Kou et al., 1993), and thus the R_{rs} at these wavelengths can be reasonably assumed as 0 sr^{-1}. For the R_{rs} spectra obtained from SeaBASS, we only downloaded those data marked as 'final' status, which indicate the R_{rs} spectra have been preprocessed (including the correction of residual reflected skylight). The quality of all R_{rs} spectra (including 114 spectra from Japanese lakes and 129 spectra from SeaBASS) was checked using a method proposed by Wei et al. (2016), which is a quality assurance (QA) system for providing a score between 0 (unusable) and 1 (perfect) to each R_{rs} spectrum to objectively evaluate its quality. In this study, only the R_{rs} spectra with quality scores larger than 0.8 were used for Z_{SD} estimations. Figure 2 shows the final remained R_{rs} spectra (84 from Japanese lakes, 94 from SeaBASS). All selected R_{rs} spectra were then converted to MERIS bands based on the MERIS Spectral Response Functions.

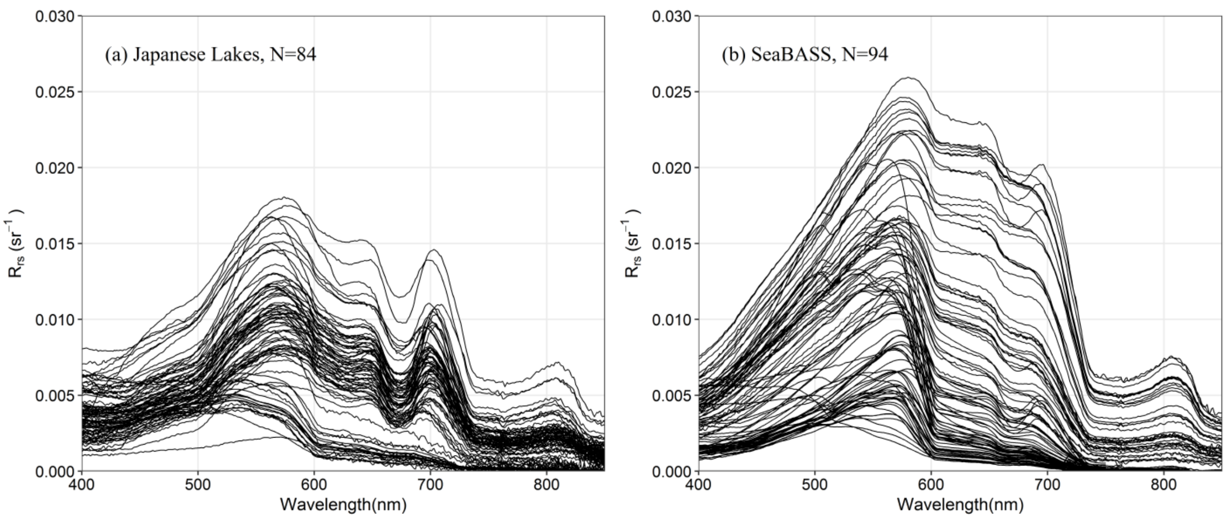

Fig.2. R_{rs} spectra used in this study. (a) 84 R_{rs} spectra collected from 8 lakes in Japan. (b) 94 R_{rs} spectra collected from SeaBASS.

For 8 Japanese lakes, water samples were collected and kept in ice boxes, and taken to the laboratory immediately after finishing the collection. The absorption coefficients of phytoplankton ($a_{ph}(\lambda)$), tripton ($a_{tr}(\lambda)$) and CDOM ($a_{CDOM}(\lambda)$) were measured following the NASA protocols (Mitchell et al., 2002). The total absorption coefficient $a(\lambda)$ was calculated as the sum of $a_{ph}(\lambda)$, $a_{tr}(\lambda)$, $a_{CDOM}(\lambda)$, and the absorption coefficient of pure water, i.e.,

$a_w(\lambda)$. The values of $a_w(\lambda)$ were taken from Lee et al. (2015b), Pope and Fry (1997), and Kou et al. (1993). In total, $a(\lambda)$ values at 52 sites from Lakes Suwa and Kasumigaura were collected.

In several Japanese lakes (Lakes Shirakaba, Unagi, Sai, Biwa, Suwa and Kasumigaura), the downward irradiance (E_d) at 443 nm, 555 nm, and 669 nm at different depths of the water column was also measured using a Multispectral Radiometer (Satlantic, Halifax, Canada). These data were used to obtain the measured K_d and then compared with R_{rs}-derived K_d at these wavelengths. In total, the measured K_d values at 99 sites were collected.

We also obtained the in situ Z_{SD} data measured between 2003 and 2012 from the Lake Kasumigaura Database, which was published by the National Institute for Environmental Studies, Japan (NIES, 2016; referred to hereafter as the 'NIES-dataset'). This database provides monthly Z_{SD} values at 10 sites in Lake Kasumigaura (the monitoring sites shown in Fig. 1b). We used these data to evaluate the performance of the proposed algorithm by using actual satellite images. For more appropriate comparison, we corrected variations of visibility due to changes in the solar zenith angle for these in situ-measured Z_{SD} values using a method proposed by Verschuur (1997).

2.3. Satellite image pre-processing

We used MERIS data in this study because of its higher spatial (300 m) and temporal (3 days') resolutions. All available MERIS images covering Lake Kasumigaura from 2003 to 2012 were downloaded from the European Space Agency (ESA, https://www.esa.int/ESA). The downloaded images were first clipped to the Lake Kasumigaura area, and then radiometric correction was performed to remove the smile-effect.

We used the Case-2 Regional Processor in the BEAM 5.0 Earth Observation Toolbox and Development Platform (Brockmann Consult, Geesthacht, Germany) to perform atmospheric correction. Clouds, cloud shadows, cloud buffers and coastal lines were then detected using the Idepix algorithm in the Sentinel Application Platform 6.0 (SNAP). Finally, the pixels with failed atmospheric correction, clouds, cloud shadows, cloud buffers, or land and coastal lines were masked out. A total of 200 images remained for the Z_{SD} estimation.

For all MERIS-derived Z_{SD} values, we firstly corrected variations of visibility due to changes in the solar zenith angle using Verschuur's method (Verschuur, 1997). We then averaged all daily estimated Z_{SD} values in the same month to generate monthly estimated Z_{SD} values. Finally, a temporal trend analysis was carried out for both monthly measured and estimated Z_{SD} values during the study period using a linear regression method, which has been widely used in previous studies (e.g., Shang et al., 2016).

Matchups were generated to compare MERIS-derived Z_{SD} values and the in situ-measured Z_{SD} values from NIES-dataset (acquired on the same day). A 3×3 window was used to extract the estimated Z_{SD} values from the MERIS images, and we used the averaged Z_{SD} estimations for the comparison to mitigate effects due to imperfect geometric corrections.

3. Development and Assessment of the Z_{SD} Retrieval Algorithm

3.1. The original Lee15 algorithm

The original Lee15 algorithm contains three main steps. First, QAA_v6 is used to retrieve $a(\lambda)$ and $b_b(\lambda)$ from $R_{rs}(\lambda)$. In the QAA_v6, if $R_{rs}(670) < 0.0015$ sr^{-1}, 560 nm is used as the reference band (i.e., QAA_v5), otherwise the reference band is shifted to 670 nm. Second, $K_d(\lambda)$ is estimated from $a(\lambda)$ and $b_b(\lambda)$ using the following equation (Lee et al., 2005, 2013):

$$K_d(\lambda) = (1 + 0.005\theta)a(\lambda) + 4.259\left(1 - 0.265\,\eta_w(\lambda)\right)\left(1 - 0.52e^{-10.8a(\lambda)}\right)b_b(\lambda) \quad (2)$$

where θ is the solar zenith angle, $\eta_w(\lambda)$ is the ratio of $b_{bw}(\lambda)$ (the backscattering coefficient of pure water, Morel, 1974; Zhang et al., 2009) and $b_b(\lambda)$. Finally, the Z_{SD} is estimated from $K_d(\lambda)$ and the corresponding $R_{rs}(\lambda)$ using the following equation based on the new underwater visibility theory (Lee et al., 2015a):

$$Z_{SD} = \frac{1}{2.5\mathrm{Min}(K_d(\lambda))}\ln\left(\frac{|0.14 - R_{rs}^{PC}|}{C_t^r}\right) \quad (3)$$

where $Min(K_d(\lambda))$ is the minimum K_d value among the visible bands, R_{rs}^{PC} is the corresponding R_{rs} at the band with the minimum K_d, and C_t^r is the contrast threshold for sighting a white disk (i.e., 0.013 sr^{-1}). The coefficient of 2.5 was obtained under an empirical assumption of $K_T = 1.5K_d$.

3.2. Improving the Lee15 algorithm for Z_{SD} retrieval in a variety of water bodies

We carried out two improvements for the original Lee15 algorithm. First, by considering the shortcoming of QAA_v6 in turbid waters, we proposed the use of another QAA, which was specifically developed for turbid inland waters by Yang et al. (2013), to estimate $a(\lambda)$ and $b_b(\lambda)$ in this type of waters (hereafter referred to as the 'QAA_T'). We selected the QAA_T algorithm in this study because all of the equations in the QAA_T are semi-analytical or analytical equations without any in situ data used for recalibration (Yang et al., 2013).

For clear waters, we still used QAA_v5 because of its good performance in this type of waters (Lee et al., 2002; Fukushima et al., 2016). We adapted the maximum chlorophyll-a index (MCI) originally developed by Gower et al. (2005) for switching the QAA_v5 and QAA_T. The modified MCI is defined as (Matsushita et al., 2015):

$$MCI = R_{rs}(709) - R_{rs}(665) - \left[\frac{(709-665)}{(754-665)}\left(R_{rs}(754) - R_{rs}(665)\right)\right] \quad (4)$$

where $R_{rs}(665)$, $R_{rs}(709)$ and $R_{rs}(754)$ are the remote sensing reflectance at 665 nm, 709 nm and 754 nm, respectively. According to Matsushita et al. (2015), MCI = 0.0016 sr^{-1} was used to distinguish clear and turbid waters. We named this blended QAA as 'QAA_hybrid', and its main steps are summarized in Table 2.

Table 2. Main steps of the QAA_hybrid

Step	Property	Derivation	
1	$r_{rs}(\lambda)$	$r_{rs}(\lambda) = R_{rs}(\lambda)/\left(0.52 + 1.7R_{rs}(\lambda)\right)$	
2	$u(\lambda)$	$u(\lambda) = \dfrac{-0.089 + \sqrt{0.089^2 + 4 \times 0.125 r_{rs}(\lambda)}}{2 \times 0.125}$	
3	MCI	$\mathrm{MCI} \leq 0.0016\ \mathrm{sr}^{-1}$ (QAA_v5)	$\mathrm{MCI} > 0.0016\ \mathrm{sr}^{-1}$ (QAA_T)
4	$a(\lambda_0)$	$x = \log\left(\dfrac{r_{rs}(443) + r_{rs}(490)}{r_{rs}(560) + 5\dfrac{r_{rs}(670)}{r_{rs}(490)}r_{rs}(670)}\right)$ $a(560) = a_w(560) + 10^{-1.146-1.366x-0.469x^2}$	$a(754) = a_w(754)$
5	$b_{bp}(\lambda_0)$	$b_{bp}(560) = \dfrac{u(560) \times a(560)}{1 - u(560)} - b_{bw}(560)$	$b_{bp}(754) = \dfrac{u(754) \times a(754)}{1 - u(754)} - b_{bw}(754)$
6	$b_{bp}(\lambda)$	$Y = 2.0\left(1 - 1.2\exp\left(-0.9\dfrac{r_{rs}(443)}{r_{rs}(560)}\right)\right)$ $b_{bp}(\lambda) = b_{bp}(560)\left(\dfrac{560}{\lambda}\right)^Y$	$Y = -372.99\beta^2 + 37.286\beta + 0.84$ $\beta = \log[u(754)/u(779)]$ $b_{bp}(\lambda) = b_{bp}(754)\left(\dfrac{754}{\lambda}\right)^Y$
7	$a(\lambda)$	$a(\lambda) = \left(1 - u(\lambda)\right)\left(b_{bw}(\lambda) + b_{bp}(\lambda)\right)/u(\lambda)$	

Our second improvement for the Lee15 algorithm was to develop another algorithm for estimating a more realistic ratio of K_T and K_d in various waters. According to previous studies, the subsurface remote sensing reflectance (r_{rs}) at optically shallow waters can be expressed as follows (Philpot, 1989; Maritorena et al., 1994; Lee et al., 1998):

$$r_{rs} \approx r_{rs}^{dp}\{1 - A_0\exp[-(K_d + K_u^C)H]\} + A_1\rho\exp[-(K_d + K_u^B)H] \tag{5}$$

where r_{rs}^{dp} is the r_{rs} for optically deep waters, A_0 is 1.0, and A_1 is $1/\pi$ for a lambertian bottom, K_u^C is the diffuse attenuation coefficient of upwelling radiance from the water column scattering, K_u^B is the diffuse attenuation coefficient of upwelling radiance from the bottom, ρ is the bottom reflectance, and H is the bottom depth. The first term on the right side of the equation refers to the reflectance from the water column, and the second term on the right refers to the reflectance from the bottom. According to Lee et al. (1999) and Barnes et al. (2018), K_d and K_u^B can be estimated using the following equations:

$$K_d = D_d \alpha \approx [1/\cos(\theta_w)]\alpha \tag{6}$$

$$K_u^B = D_u^B \alpha \approx [1.04(1+5.4u)^{0.5}]\alpha \tag{7}$$

where θ_w is the subsurface solar zenith angle, α is defined as $(a+b_b)$, and u is defined as $b_b/(a+b_b)$. If we treat the bottom of the water as the Secchi disk, and assume that the disk is a lambertian object, then the second term on the right side of Eq. (5) becomes the light that comes from the Secchi disk. Therefore, the K_u^B can be considered to be the K_T in the new Z_{SD} theory (i.e., $K_T = K_u^B$). By converting the subsurface solar zenith angle θ_w to the above surface solar zenith angle θ, and combining the Eqs. (6) and (7), the ratio of K_T and K_d can be expressed as:

$$K_T/K_d = \frac{1.04(1+5.4u)^{0.5}}{1/\left(1-\frac{\sin(\theta)^2}{RI^2}\right)^{0.5}} \tag{8}$$

where RI is the refractive index value of the water (1.34, Lee et al., 1998). By replacing the fixed value of 2.5 in Eq. (3) with (1+K_T/K_d), the Lee15 algorithm can be modified as:

$$Z_{SD} = \frac{1}{(1+K_T/K_d)\cdot \mathrm{Min}(K_d(\lambda))} \ln\left(\frac{|0.14-R_{rs}^{PC}|}{C_t^r}\right) \tag{9}$$

3.3. Accuracy assessment

We used the root mean square error (RMSE), the mean absolute percentage error (MAPE), and bias to evaluate the performance of the improved Lee15 algorithm. The equations are as follows:

$$RMSE = \sqrt{\frac{\sum_{i=1}^{N}\left(X_{estimated,i} - X_{measured,i}\right)^2}{N}} \quad (10)$$

$$MAPE = \frac{1}{N}\sum_{i=1}^{N}\left|\frac{X_{estimated,i} - X_{measured,i}}{X_{measured,i}}\right| \cdot 100\% \quad (11)$$

$$Bias = \frac{1}{N}\sum_{i=1}^{N}\left(X_{estimated,i} - X_{measured,i}\right) \quad (12)$$

where $X_{estimated}$ is the estimated parameter (e.g., a, K_d or Z_{SD}), $X_{measured}$ is the corresponding in situ measurement, and N is the number of data. The determination coefficient (R^2) was also calculated for reference.

4. **Results**

4.1. The a, K_d and Z_{SD} values estimated from in situ R_{rs} spectra

Figure 3 shows the results of our comparisons of the derived $a(\lambda)$ and in situ $a(\lambda)$ at all MERIS visible bands. It can be seen that the QAA_v6 gave larger underestimations of $a(\lambda)$ at all visible bands, with RMSE = 1.82 m^{-1}, MAPE = 59% and Bias = −1.29 m^{-1} (Fig. 3a). In contrast, the QAA_hybrid showed better retrievals of $a(\lambda)$ at all visible bands with RMSE = 0.77 m^{-1}, MAPE = 22% and Bias = −0.30 m^{-1} (Fig. 3b). The determination coefficient was also increased from 0.66 to 0.79. However, some retrieved absorption coefficients at 443 nm (data collected from Lake Kasumigaura on April 18, 2016) still showed slight underestimations.

We checked the bands corresponding to the minimum K_d and found that 443 nm was not selected for Z_{SD} estimations. If we compare only the retrieved $a(\lambda)$ and the in situ $a(\lambda)$ at the selected bands (i.e., the band with minimum K_d in visible domain and finally used for Z_{SD} estimations), no obvious underestimations or overestimations from the use of QAA_hybrid were observed (Fig. 3d), whereas the QAA_v6 still showed larger underestimated $a(\lambda)$ at the selected bands (Fig. 3c). The values of RMSE, MAPE, Bias, and R^2 were calculated as 0.23 m^{-1}, 19%, −0.04 m^{-1}, and 0.65, respectively, with the use of the QAA_hybrid at the selected bands.

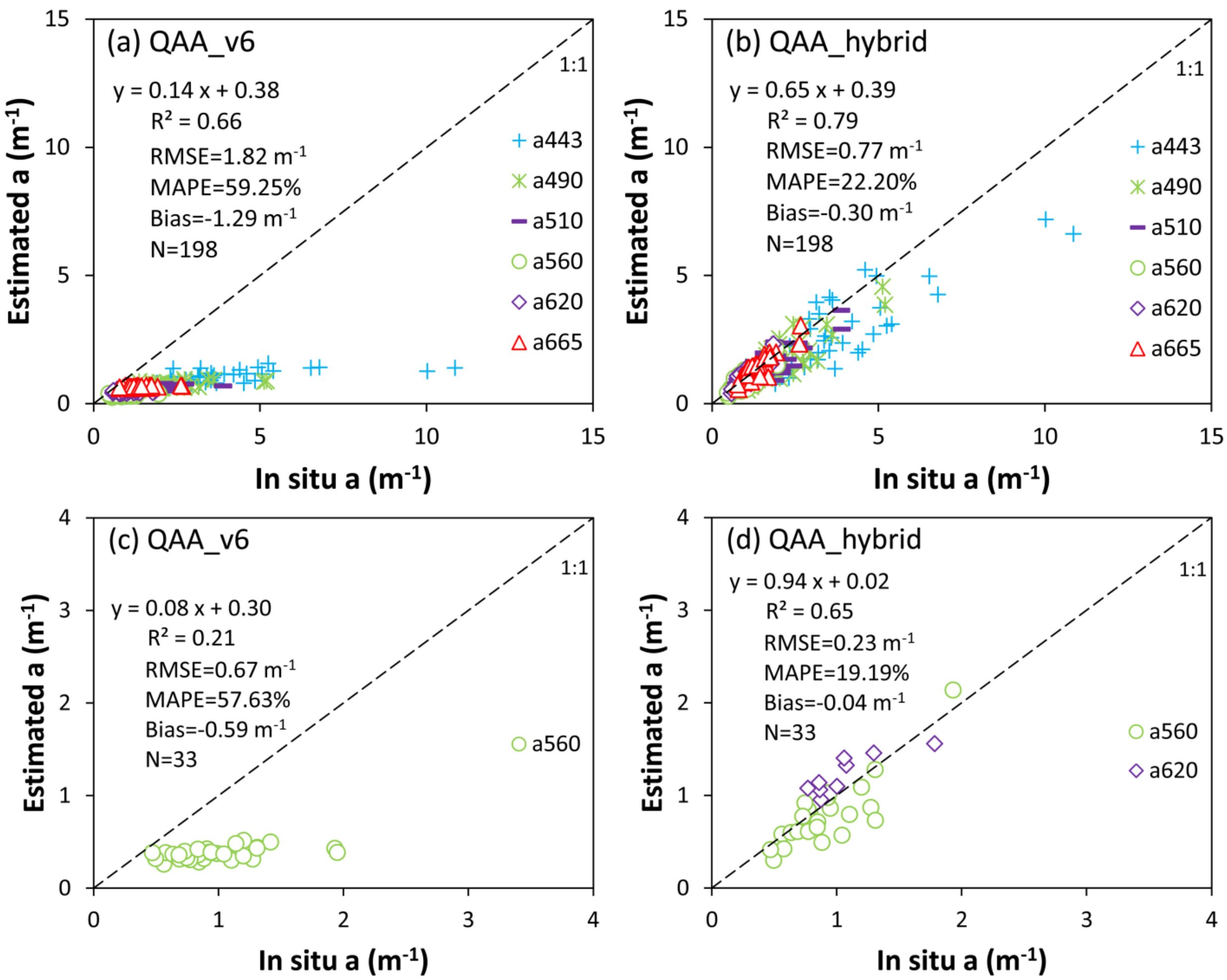

Fig. 3. Comparison between in situ absorption coefficients and estimated absorption coefficients,

estimated using (a) QAA_v6 at all MERIS visible bands, (b) QAA_hybrid at all MERIS visible bands, (c) QAA_v6 only at the bands corresponding to the minimum K_d values, and (d) the QAA_hybrid only at the bands corresponding to the minimum K_d values.

Figure 4 illustrates the results of our comparisons of the retrieved K_d and the in situ-measured K_d at 443, 555 and 669 nm. It can be seen that using $a(\lambda)$ and $b_b(\lambda)$ estimated from the QAA_v6 resulted in large underestimations of K_d (RMSE = 2.33 m^{-1}, MAPE = 54% and Bias = −1.73 m^{-1}, Fig. 4a), and these underestimations were largely improved by using the QAA_hybrid instead of QAA_v6 (RMSE = 0.93 m^{-1}, MAPE = 24% and Bias = −0.44m^{-1}, Fig. 4b). We also compared only the K_d at the bands finally used for the Z_{SD} estimations (i.e., the minimum K_d) and the corresponding in situ-measured K_d; similar improvements were found by comparing the use of $a(\lambda)$ and $b_b(\lambda)$ obtained from QAA_v6 with those obtained using the QAA_hybrid (Fig. 4c, d). It should be noted that the smaller numbers of data in Fig. 4c and Fig. 4d are because the estimated minimum K_d values were found at wavelengths without in situ measurements for some sampling sites.

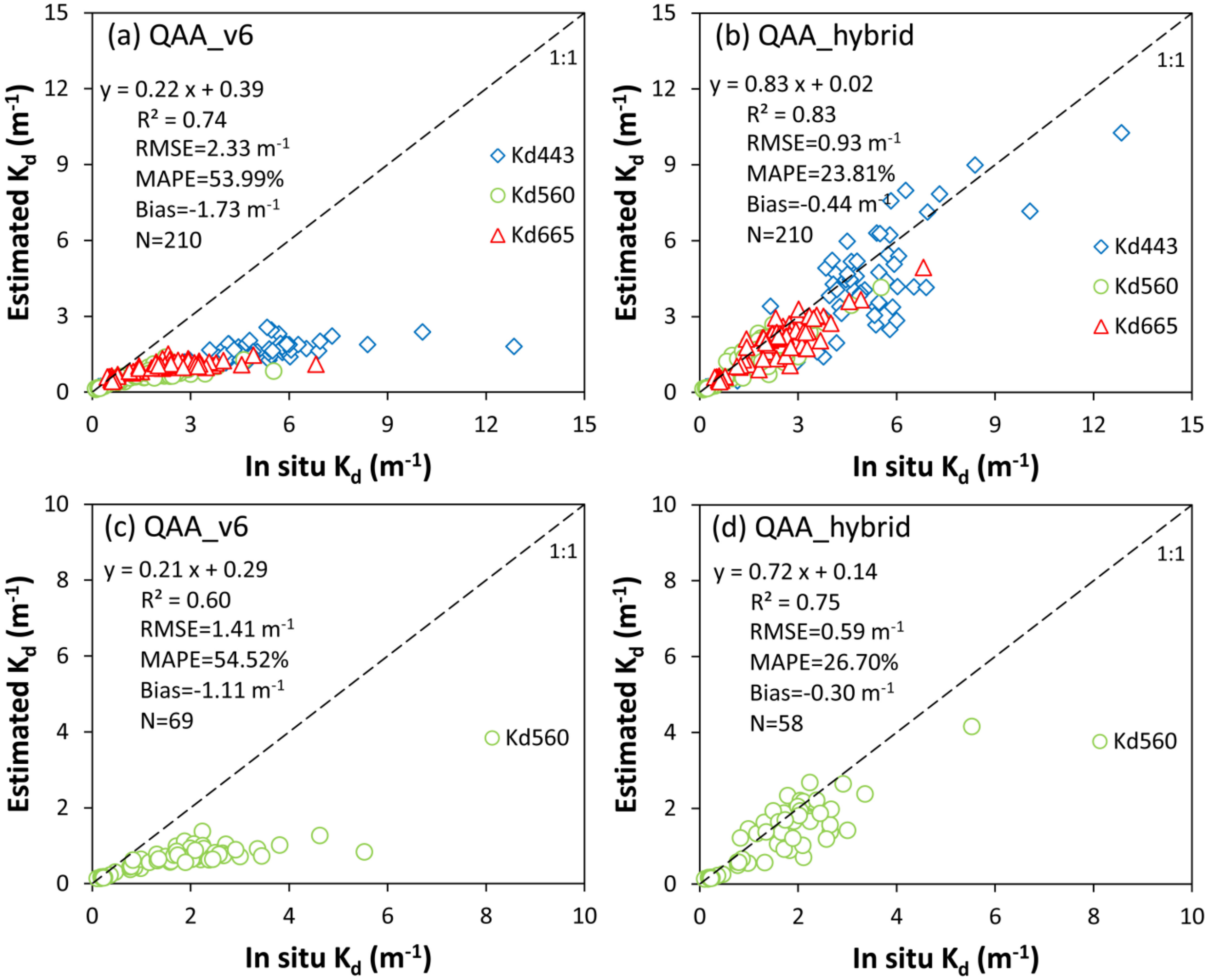

Fig.4. Comparison between in situ-measured K_d and estimated K_d at bands of 443 nm, 560 nm and 665 nm. (a) Estimated $K_d(\lambda)$ using $a(\lambda)$ and $b_b(\lambda)$ from QAA_v6. (b) Estimated $K_d(\lambda)$ using $a(\lambda)$ and $b_b(\lambda)$ from the QAA_hybrid. (c) Only the estimated K_d at the minimum K_d bands using $a(\lambda)$ and $b_b(\lambda)$ from QAA_v6. (d) Only the estimated K_d at the minimum K_d bands using $a(\lambda)$ and $b_b(\lambda)$ from the QAA_hybrid.

Figure 5 shows the estimated K_T/K_d ratios obtained using Eq. (8) for all available data

(N=178). The results showed that the K_T/K_d ratios ranged from 0.91 to 1.64 with an average value of 1.24. These ratios were different from the fixed value of 1.5 used in the original Lee15 algorithm. In addition, the K_T/K_d ratios of clear waters (i.e., Z_{SD} values ≥ 2 m) were significantly lower than those of turbid waters (i.e., Z_{SD} values < 2 m), with a mean K_T/K_d ratio of 1.16 in clear waters and 1.30 in turbid waters (P < 0.001).

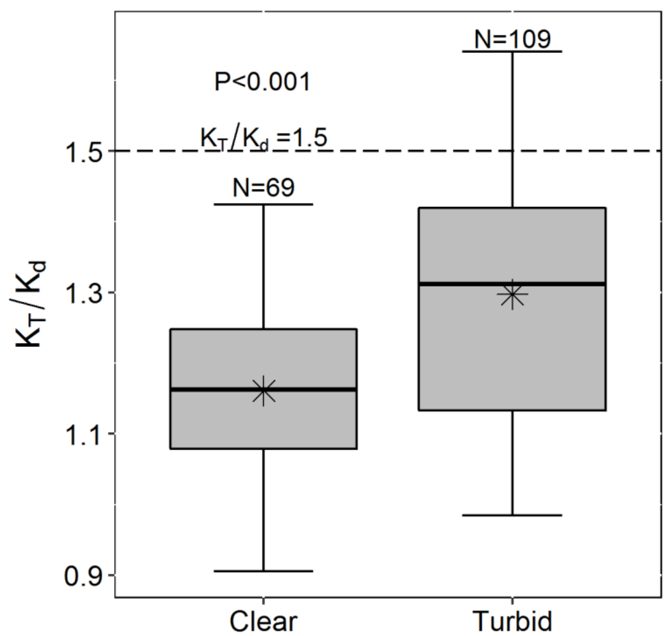

Fig. 5. Comparison of estimated K_T/K_d values between clear (Z_{SD} values ≥2 m) and turbid (Z_{SD} values <2 m) waters. *Black star:* The mean K_T/K_d ratio. *Dashed line:* $K_T/K_d = 1.5$, which was used in the original Lee15 algorithm.

Figure 6 shows the results of our comparisons of the estimated and in situ-measured Z_{SD} values. The results showed that: (1) the original Lee15 algorithm clearly underestimated the Z_{SD}

in clear waters (solid symbols) and overestimated the Z_{SD} in turbid waters (hollow symbols), with the RMSE of 0.18 in log10 unit and MAPE of 39% (Fig. 6a); (2) the overestimations in turbid waters were improved by using the QAA_hybrid instead of QAA_v6, with a reduced RMSE of 0.14 in log10 unit and MAPE of 23% (Fig. 6b; hollow symbols); (3) the underestimations in clear waters were much improved by using dynamic K_T/K_d ratios instead of the constant ratio of 1.5, even with slightly increased RMSE of 0.19 in log10 unit and MAPE of 45% (Fig. 6c; solid symbols); and (4) both overestimations and underestimations were improved by combining the QAA_hybrid and dynamic K_T/K_d ratios, with a reduced RMSE of 0.11 in log10 unit and MAPE of 20% (Fig. 6d). The slope and intercept values of the regression lines were also changed from 0.70 to 0.89 and from 0.59 to 0.13, respectively.

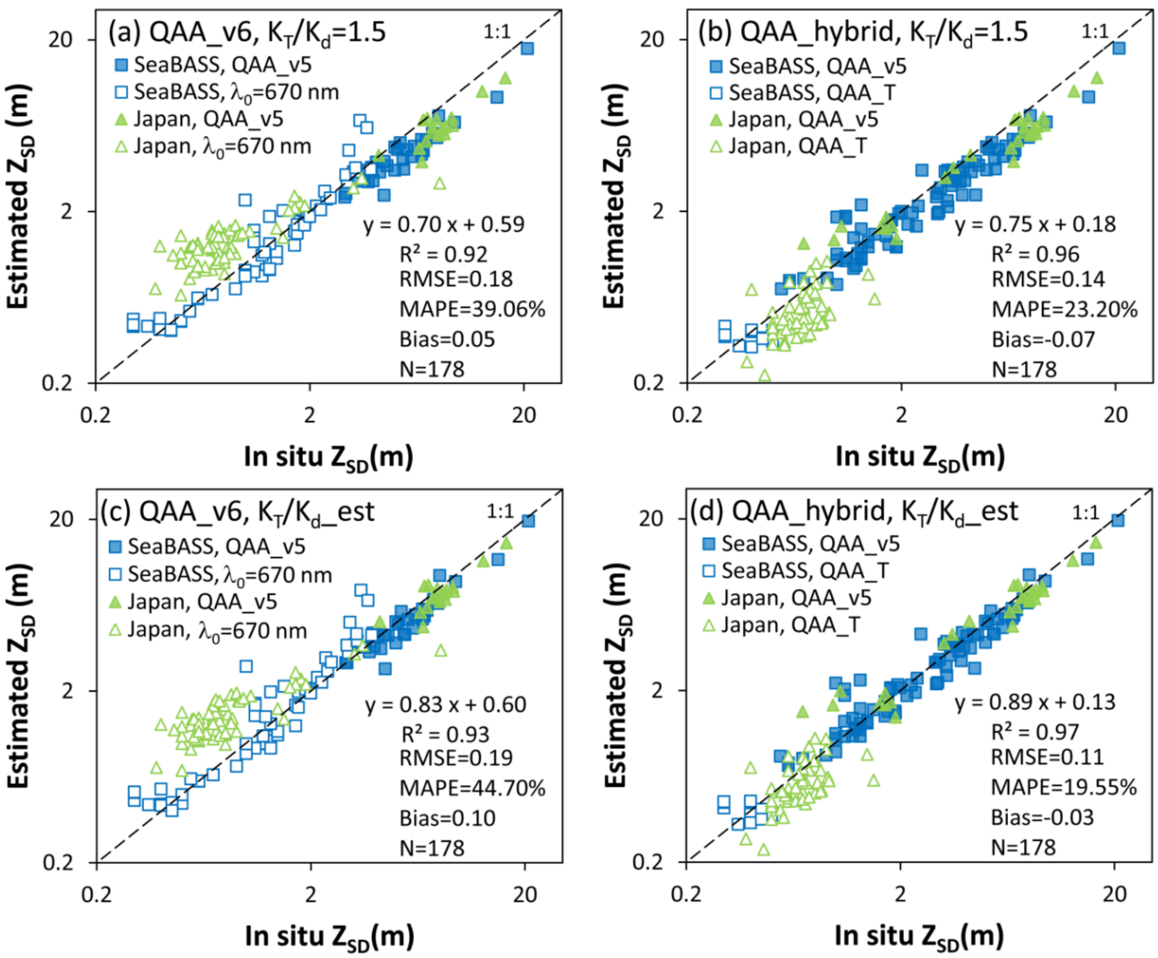

Fig. 6. Comparisons between in situ measured Z_{SD} values and estimated Z_{SD} values from in situ R_{rs}. (a) Estimated Z_{SD} based on QAA_v6 with $K_T/K_d = 1.5$ (i.e., original Lee15 algorithm). (b) Estimated Z_{SD} based on the QAA_hybrid but still with $K_T/K_d = 1.5$. (c) Estimated Z_{SD} based on QAA_v6 but with dynamic K_T/K_d ratios (K_T/K_d_est). (d) Estimated Z_{SD} based on the QAA_hybrid with dynamic K_T/K_d ratios (i.e., the improved Lee15 algorithm). Solid symbols represent the Z_{SD} estimated using 560 nm as reference band in both QAA_v6 and QAA_hybrid (i.e., QAA_v5), and hollow symbols represent the Z_{SD} estimated using 670 nm as reference band in QAA_v6 and using 754 nm as reference band in QAA_hybrid (i.e., QAA_T).

4.2. Z_{SD} estimated from MERIS data in Lake Kasumigaura

Figure 7 shows the comparisons of the estimated Z_{SD} values from actual MERIS data and the in situ-measured Z_{SD} values for 19 matchups (with time windows ≤ 4 hours and differences of solar zenith angles ≤ 9 degree). Similar to the results showed in Figure 6, the improved Lee15 algorithm achieved the best performance with the smallest RMSE of 0.11 m, MAPE of 15%, and the highest determination coefficient of 0.58 (Fig. 7d). The original Lee15 algorithm overestimated the Z_{SD} in Lake Kasumigaura (Fig. 7a). These overestimations were improved mainly by using the QAA_hybrid instead of QAA_v6 (Fig. 7b, with the RMSE reduced from 0.54 m to 0.15 m and the MAPE reduced from 76% to 20%). Figure 7c shows that only using the dynamic K_T/K_d ratios instead of the constant ratio of 1.5 resulted in decreased estimation accuracy with the largest RMSE (0.72 m) and MAPE (99%) values, but improved determination coefficient (from 0.49 to 0.54).

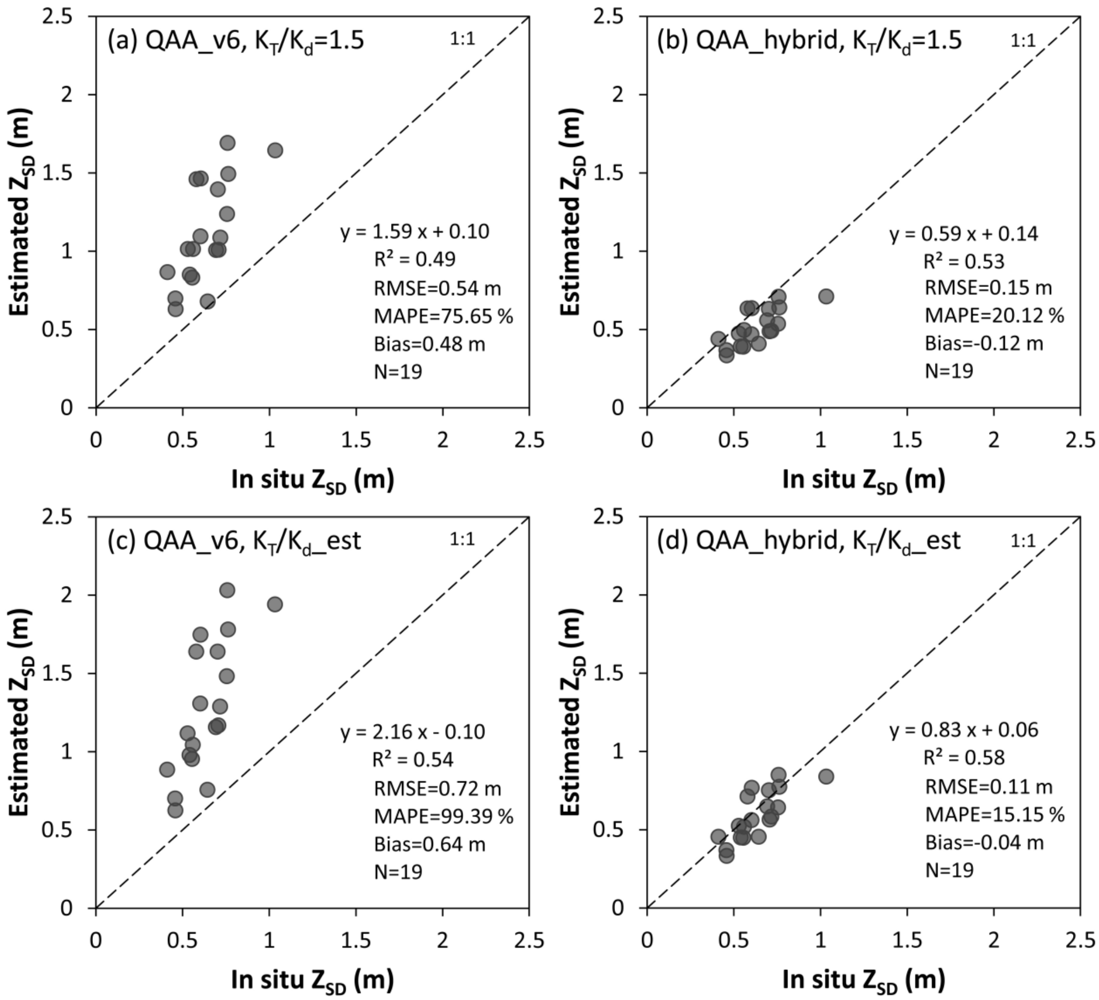

Fig. 7. Comparisons of the in situ Z_{SD} and estimated Z_{SD} values from MERIS data. (a) Estimated Z_{SD} using QAA_v6 with $K_T/K_d = 1.5$ (i.e., the original Lee15 algorithm). (b) Estimated Z_{SD} using the QAA_hybrid but still with $K_T/K_d = 1.5$. (c) estimated Z_{SD} using QAA_v6 but with dynamic K_T/K_d ratios (K_T/K_d_est). (d) Estimated Z_{SD} using the QAA_hybrid with dynamic K_T/K_d ratios (i.e., the improved Lee15 algorithm).

Figure 8 shows the comparisons of the monthly measured and estimated Z_{SD} values in

Lake Kasumigaura for a long-term period (2003–2012). The monthly measured Z_{SD} values were obtained from the NIES-dataset, and the monthly estimated Z_{SD} values were obtained from the available MERIS data between 2003 and 2012 using the original Lee algorithm and the improved Lee15 algorithm. Sites 1, 2 and 6 of Lake Kasumigaura were excluded from the comparison because they are too close to the shoreline and strongly influenced by the land (i.e. no any available estimated Z_{SD} values within the 3×3 windows after one pixel buffer from shoreline was removed). In total, we obtained 200 MERIS images; however, because a few sites were covered by clouds, cloud shadows, or not covered by MERIS images (Lake Kasumigaura was partly covered by one MERIS image), there were the following numbers of available MERIS images for the sites: 122 images for site 3; 72 images for site 4; 114 images for site 7; 135 images for site 8; 138 images for site 9; 133 images for site 11; and 124 images for site 12.

Overall, the temporal trends of Z_{SD} values obtained from MERIS data by using the improved Lee15 algorithm (red line with triangles) agreed well with those obtained from field surveys (blue line with circles) at all seven sites. Both the monthly estimated Z_{SD} values using the improved Lee15 algorithm and the monthly in situ-measured Z_{SD} values showed a significant increase trend in Lake Kasumigaura during the 10-year study period (with all slopes > 0 and all P values < 0.001). In contrast, the estimated Z_{SD} using the original Lee15 algorithm showed obvious overestimations and lower R^2 values in the temporal trend analyses (green line with diamonds).

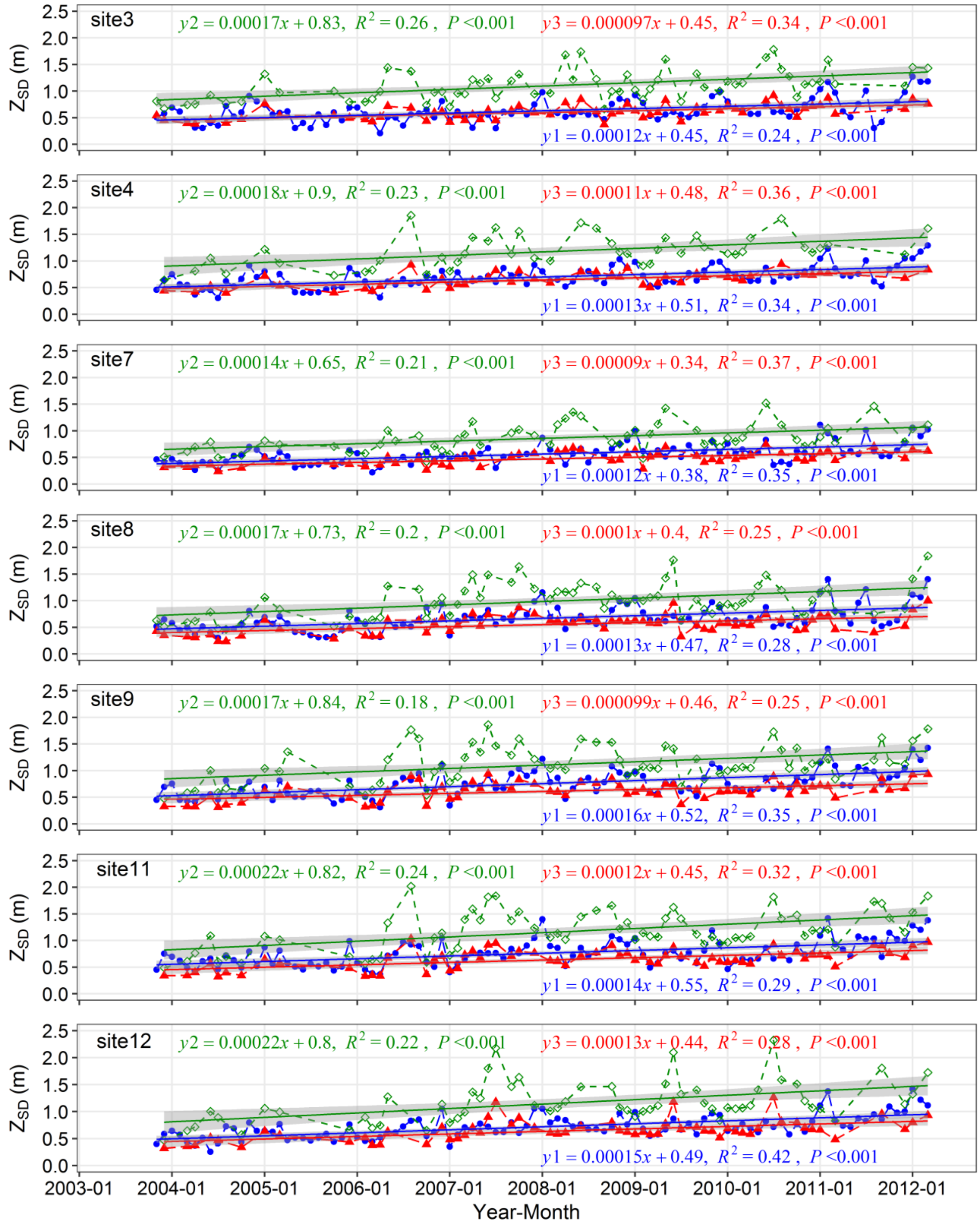

Fig. 8. Monthly Z_{SD} changes from 2003 to 2012 at seven sites in Lake Kasumigaura. Blue dashed line with solid circles represents monthly in situ-measured Z_{SD} values, and blue solid line

represents temporal trend obtained from the monthly in situ-measured Z_{SD} values (y1); red dashed line with solid triangles represents monthly mean MERIS-derived Z_{SD} values using the improved Lee15 algorithm, and red solid line represents temporal trend obtained from the monthly mean MERIS-derived Z_{SD} values using the improved Lee15 algorithm (y3); green dashed line with hollow diamonds represents monthly mean MERIS-derived Z_{SD} values using the original Lee15 algorithm, and green solid line represents temporal trend obtained from the monthly mean MERIS-derived Z_{SD} values using the original Lee15 algorithm (y2).

5. Discussion

5.1. Necessity of the QAA_hybrid

The estimations of $a(\lambda)$ and $b_b(\lambda)$ using QAA_v6 is the first step in the original Lee15 algorithm (Lee et al., 2015a). Both previous studies and our results have confirmed that the estimation errors that occur in this step will be propagated to the $K_d(\lambda)$ estimations in the second step and then the Z_{SD} estimations in the final step (Yang et al., 2014, 2015; Figs. 3a, 4a, and 6a in this study). Failures of QAA_v6 applications usually occurred in turbid waters (Yang et al., 2014; Wang et al., 2017; Rodrigues et al., 2017). It is thus necessary to use an alternative to QAA_v6 for turbid waters.

Although several modified QAAs have been proposed for retrieving $a(\lambda)$ and $b_b(\lambda)$

values in turbid waters, two empirical relationships for estimating the absorption coefficient at a reference band ($a(\lambda_0)$, step 4 in Table 2) and the spectral slope of the backscattering coefficient of suspended particles (Y, step 6 in Table 2) must be recalibrated by using in situ data in most of these modified QAAs (Le et al., 2009; Huang et al., 2014; Mishra et al., 2014; Wang et al., 2017). The constant requirement of in situ data for model recalibration will make the two empirical relationships the first important equations in these modified QAAs, and thus will limit their applicability in various waters. In contrast, QAA_T proposed by Yang et al. (2013) does not include empirical equations for $a(\lambda)$ and $b_b(\lambda)$ retrievals, and thus it is the most proper algorithm to replace QAA_v6 for retrieving $a(\lambda)$ and $b_b(\lambda)$ in turbid waters (Yang et al., 2014, 2015; Fukushima et al., 2016).

However, QAA_T did not work well in clear waters. For example, if we used QAA_T to retrieve $a(\lambda)$ and $b_b(\lambda)$ for waters with an in situ $Z_{SD} \geq 2$ m (there are 69 such points in Fig. 6), larger errors occurred in the estimated Z_{SD} values with the RMSE of 5.24 m, the MAPE of 77%, and the very low determination coefficient of 0.01 (data not shown). In contrast, QAA_v5 performed very well for these points with the RMSE of 1.01 m, the MAPE of 14%, and the determination coefficient of 0.94.

In QAA_hybrid, we selected QAA_v5 for clear waters rather than QAA_v6. This is because that we found QAA_v5 outperformed QAA_v6 in our dataset. Figure 9 shows the comparison of the estimated Z_{SD} values using QAA_v5 and using QAA_v6 for 59 R_{rs} spectra. The 59 R_{rs} spectra were selected by using the criteria of MCI ≤ 0.0016 sr^{-1} and $R_{rs}(670) > 0.0015$ sr^{-1}. In other words, the 59 R_{rs} spectra would select 670 nm as reference band if we used QAA_v6 instead of QAA_v5 for clear waters. In contrast, all R_{rs} spectra with MCI ≤ 0.0016 sr^{-1} (111 R_{rs} spectra in total) only used 560 nm as reference band in QAA_hybrid. From Figure 9, it can be seen that QAA_v5 (left) performed better than QAA_v6 (right) with the RMSE reduced from 1.06 m to 0.53 m, the MAPE reduced from 29% to 23%, and the R^2 increased from 0.49 to 0.80. The above findings indicate that it is necessary to select the appropriate QAA according to water turbidities. In other words, it is necessary to use a hybrid QAA to address various waters.

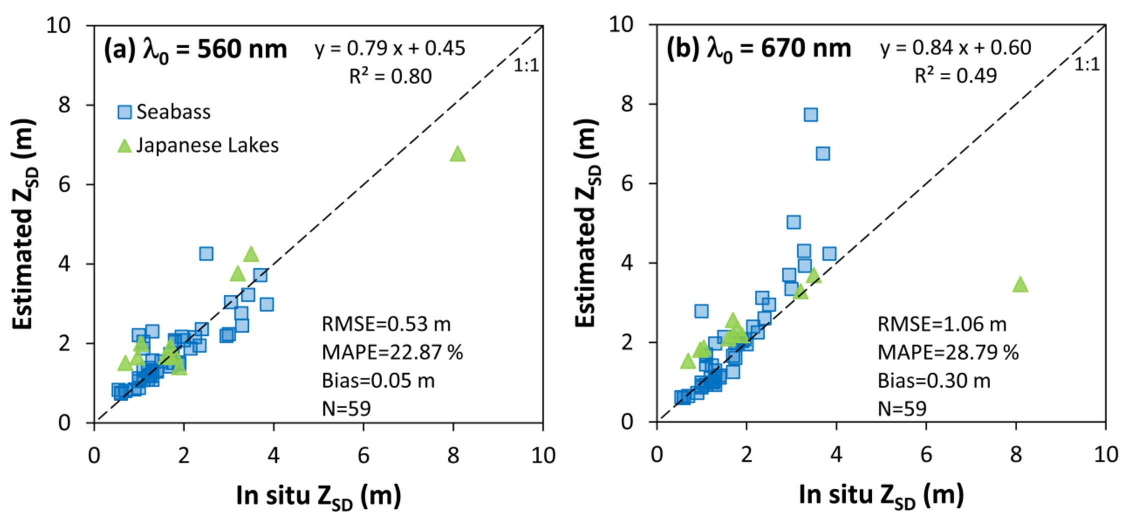

Fig. 9. Comparisons between in situ-measured Z_{SD} values and corresponding estimated Z_{SD} values from 59 selected in situ R_{rs} (see text for details). (a) using 560 nm as reference band; (b) using 670 nm as reference band.

In this study, we used MCI = 0.0016 sr^{-1} to switch QAA_v5 and QAA_T. This MCI threshold was suggested by Matsushita et al. (2015) based on the data collected from five Asian lakes (Lake Erhai and Lake Dianchi in China; Lake Biwa, Lake Suwa, and Lake Kasumigaura in Japan). Our present findings also demonstrated that this threshold is reasonable. Other information can also be used to select the appropriate QAA. For example, Moore et al. (2014) proposed a method to classify waters into seven optical water types (OWTs); Spyrakos et al. (2018) identified 13 OWTs for inland waters based on comprehensive data from more than 250 aquatic systems. Further study is needed to compare the performances of different water classification algorithms for selecting the most appropriate QAAs.

5.2. The importance of the estimation of the K_T/K_d ratio

The reported K_T/K_d ratios range from 0.5 to 2.0 (Philpot, 1989; Maritorena et al., 1994; Lee et al., 1994). In the present study, the K_T/K_d ratios were estimated in the range of 0.91–1.64 with an average of 1.24 (Fig. 5). This range is similar to that reported by Maritorena et al. (1994) with K_T/K_d ratios between 1.02 and 1.66. Our results also showed that the K_T/K_d ratios in clear waters are significantly smaller than those in turbid waters (Fig. 5, $p<0.001$). This finding agrees with Philpot (1989), who reported that the K_T/K_d ratios tended to be higher in strongly absorbing waters.

Compared to the K_T/K_d ratios in turbid waters (with a mean ratio of 1.30), the K_T/K_d ratios in clear waters (with a mean ratio of 1.16) are far smaller than the constant K_T/K_d ratio of 1.5 used in the original Lee15 algorithm. The above findings indicate that the use of the constant K_T/K_d ratio of 1.5 will lead to larger underestimations of the Z_{SD} in clear waters. For example, in Lake Motosu, a clear Japanese lake with the in situ-measured Z_{SD} of 16.4 m, the K_T/K_d ratio was estimated to be 1.06 by using Eq. (8); the estimated Z_{SD} using the original Lee15 algorithm was 12.01 m with a relative error of 26.8% (Fig. 6a), and this error was reduced to 11.2% by using the improved Lee15 algorithm (the estimated $Z_{SD} = 14.58$ m, Fig. 6d). Even in a turbid Japanese lake, i.e., Lake Kasumigaura, the use of dynamic K_T/K_d ratios also improved the Z_{SD} estimations (Fig. 7b vs. Fig. 7d).

Although our results have confirmed that the use of the dynamic K_T/K_d ratios can improve Z_{SD} estimations in both clear and turbid waters, further study is still needed to evaluate the relationship between K_T and K_d in various waters due to the Eq. (8) is based on an assumption of treating a Secchi disk as a lambertian bottom.

5.3. Applicability of the improved Lee15 algorithm

Similar to the original Lee15 algorithm, the improved Lee15 algorithm does not require any in situ data for recalibration. This is because both the QAA_hybrid (the combination of QAA_v5 and QAA_T) and the equation for estimating K_T/K_d ratios (i.e., Eq. (8)) are designed as only using semi-analytical equations, which indicates that the assumptions and empirical equations are all of secondary importance for Z_{SD} retrievals (Lee et al., 1998, 2002, 2015a; Yang et al., 2013). Therefore, although we validated the improved Lee15 algorithm by using only the data collected from 8 Japanese lakes and SeaBASS dataset, it is apparent that the algorithm can also be applied for Z_{SD} estimations in other waters worldwide.

Since both the original and improved Lee15 algorithms used only a single band for Z_{SD} retrieval (i.e., the band with the minimum K_d), an accurate algorithm for atmospheric correction is crucial when actual satellite data are used. For clear waters, the atmospheric correction algorithm proposed by Gordon and Wang (1994) will be the best choice, whereas for turbid waters, although there are several algorithms (e.g., Ruddick et al., 2000; Wang and Shi, 2007; Guanter et al., 2007; Doerffer and Schiller, 2008; Bailey et al., 2010; Jaelani et al., 2015), it is still not clear which is the most appropriate algorithm for atmospheric correction. Our present results showed that the Case-2 Regional Processor proposed by Doerffer and Schiller (2008) can be an option for turbid inland waters such as Lake Kasumigaura (Fig. 7). Further validations obtained by using more comprehensive datasets should be carried out in the future to further confirm the above considerations.

6. Conclusions

The original Lee15 algorithm showed overestimations of Z_{SD} values in turbid waters and underestimations of Z_{SD} values in clear waters. In the present study, the use of QAA_hybrid instead of QAA_v6 mainly overcame the former shortcoming through blending QAA_T and QAA_v5 for estimating more accurate absorption and backscattering coefficients in both turbid (QAA_T) and clear waters (QAA_v5); and the use of the dynamic K_T/K_d ratios instead of using the fixed K_T/K_d ratio (i.e., 1.5) mainly overcame the latter shortcoming in the original Lee15 algorithm. Our results show that the improved Lee15 algorithm gave more accurate Z_{SD} estimations, with RMSE reduced from 0.18 to 0.11 (in log10 unit) and MAPE reduced from 39% to 20% for using the in situ R_{rs} values from 8 Japanese lakes (Z_{SD} values ranged from 0.4 m to 16.4 m, N=84) and SeaBASS dataset (Z_{SD} values ranged from 0.3 m to 20.8 m, N=94). The improved Lee15 algorithm is expected to estimate more accurate Z_{SD} values in various types of waters.

Acknowledgements

This research was supported in part by the Grants-in-Aid for Scientific Research of MEXT from Japan (No. 17H01850 and No. 17H04475A), and Kurita Water and Environment Foundation Grant (18B048). We thank the European Space Agency (ESA) for providing MERIS satellite data, and the National Institute for Environmental Studies (NIES) for providing monitoring data on Z_{SD}. The authors would also like to thank two anonymous reviewers for their valuable comments and suggestions for improving the quality of the manuscript.

References

Alikas, K., & Kratzer, S. (2017). Improved retrieval of Secchi depth for optically-complex waters using remote sensing data. *Ecological Indicators*, 77, 218-227. https://doi.org/10.1016/j.ecolind.2017.02.007.

Bailey, S. W., Franz, B. A., & Werdell, P. J. (2010). Estimation of near-infrared water-leaving reflectance for satellite ocean color data processing. *Optics express*, *18*(7), 7521-7527. https://doi.org/10.1364/OE.18.007521.

Barnes, B. B., Garcia, R., Hu, C., & Lee, Z. (2018). Multi-band spectral matching inversion algorithm to derive water column properties in optically shallow waters: An optimization of parameterization. *Remote Sensing of Environment*, *204*, 424-438. https://doi.org/10.1016/j.rse.2017.10.013.

Carlson, R. E. (1977). A trophic state index for lakes. *Limnology and oceanography*, 22(2), 361-369. https://doi.org/10.4319/lo.1977.22.2.0361.

Chen, Z., Muller-Karger, F. E., & Hu, C. (2007). Remote sensing of water clarity in Tampa Bay. *Remote Sensing of Environment*, 109(2), 249-259. https://doi.org/10.1016/j.rse.2007.01.002.

Doerffer, R., and Schiller, H., 2008. MERIS Regional Coastal and Lake Case 2 Water Project - Atmospheric Correction ATBD. GKSS Research Center 21502 Geesthacht Version 1.0 18. May 2008.

Doron, M., Babin, M., Hembise, O., Mangin, A., & Garnesson, P. (2011). Ocean transparency from space: Validation of algorithms estimating Secchi depth using MERIS, MODIS and SeaWiFS data. *Remote Sensing of Environment*, *115*(12), 2986-3001. https://doi.org/10.1016/j.rse.2011.05.019.

Duntley, S. Q. (1952). The visibility of submerged objects. *Visibility Lab., Mass. Inst. Tech* (pp. 74). San Diego: Scripps Institution of Oceanography.

Fukushima, T., Matsushita, B., Oyama, Y., Yoshimura, K., Yang, W., Terrel, M., ... & Takegahara, A. (2016). Semi-analytical prediction of Secchi depth using remote-sensing reflectance for lakes with a wide range of turbidity. *Hydrobiologia*, *780*(1), 5-20. https://doi.org/10.1007/s10750-015-2584-7.

Fukushima, T., Matsushita, B., Yang, W., & Jaelani, L. M. (2018). Semi-analytical prediction of Secchi depth transparency in Lake Kasumigaura using MERIS data. *Limnology*, *19*(1), 89-100. https://doi.org/10.1007/s10201-017-0521-3.

Giardino, C., Pepe, M., Brivio, P. A., Ghezzi, P., & Zilioli, E. (2001). Detecting chlorophyll, Secchi disk depth and surface temperature in a sub-alpine lake using Landsat imagery.

Science of the Total Environment, 268(1-3), 19-29. https://doi.org/10.1016/S0048-9697(00)00692-6.

Gordon, H. R., & Wang, M. (1994). Retrieval of water-leaving radiance and aerosol optical thickness over the oceans with SeaWiFS: a preliminary algorithm. *Applied optics*, *33*(3), 443-452. https://doi.org/10.1364/AO.33.000443.

Gower, J., King, S., Borstad, G., & Brown, L. (2005). Detection of intense plankton blooms using the 709 nm band of the MERIS imaging spectrometer. *International Journal of Remote Sensing*, *26*(9), 2005-2012. https://doi.org/10.1080/01431160500075857.

Guanter, L., Del Carmen González-Sanpedro, M., & Moreno, J. (2007). A method for the atmospheric correction of ENVISAT/MERIS data over land targets. *International Journal of Remote Sensing*, *28*(3-4), 709-728. https://doi.org/10.1080/01431160600815525.

Huang, J., Chen, L., Chen, X., Tian, L., Feng, L., Yesou, H., & Li, F. (2014). Modification and validation of a quasi-analytical algorithm for inherent optical properties in the turbid waters of Poyang Lake, China. *Journal of Applied Remote Sensing*, *8*(1), 083643. https://doi.org/10.1117/1.JRS.8.083643.

IOCCG. Update of the Quasi-Analytical Algorithm (QAA_v6). IOCCG, 2014. Available online: http://www.ioccg.org/groups/Software_OCA/QAA_v6_2014209.pdf.

Jaelani, L. M., Matsushita, B., Yang, W., & Fukushima, T. (2015). An improved atmospheric correction algorithm for applying MERIS data to very turbid inland waters. *International Journal of Applied Earth Observation and Geoinformation*, *39*, 128-141. https://doi.org/10.1016/j.jag.2015.03.004.

Kabbara, N., Benkhelil, J., Awad, M., & Barale, V. (2008). Monitoring water quality in the coastal area of Tripoli (Lebanon) using high-resolution satellite data. *ISPRS Journal of Photogrammetry and Remote Sensing*, 63(5), 488-495. https://doi.org/10.1016/j.isprsjprs.2008.01.004.

Kloiber, S. M., Brezonik, P. L., Olmanson, L. G., & Bauer, M. E. (2002). A procedure for regional lake water clarity assessment using Landsat multispectral data. *Remote sensing of Environment*, 82(1), 38-47. https://doi.org/10.1016/S0034-4257(02)00022-6.

Kou, L., Labrie, D., & Chylek, P. (1993). Refractive indices of water and ice in the 0.65-to 2.5-μm spectral range. *Applied optics*, *32*(19), 3531-3540. https://doi.org/10.1364/AO.32.003531.

Kratzer, S., Brockmann, C., & Moore, G. (2008). Using MERIS full resolution data to monitor coastal waters—A case study from Himmerfjärden, a fjord-like bay in the northwestern Baltic Sea. *Remote Sensing of Environment*, 112(5), 2284-2300. https://doi.org/10.1016/j.rse.2007.10.006.

Kratzer, S., Håkansson, B., & Sahlin, C. (2003). Assessing Secchi and photic zone depth in the

Baltic Sea from satellite data. *AMBIO: A Journal of the Human Environment*, 32(8), 577-585. https://doi.org/10.1579/0044-7447-32.8.577.

Le, C. F., Li, Y. M., Zha, Y., Sun, D., & Yin, B. (2009). Validation of a quasi-analytical algorithm for highly turbid eutrophic water of Meiliang Bay in Taihu Lake, China. *IEEE Transactions on Geoscience and Remote Sensing*, *47*(8), 2492-2500. https://doi.org/10.1109/TGRS.2009.2015658.

Lee, Z. P., Du, K. P., & Arnone, R. (2005). A model for the diffuse attenuation coefficient of downwelling irradiance. *Journal of Geophysical Research: Oceans*, *110*(C2). https://doi.org/10.1029/2004JC002275.

Lee, Z., Carder, K. L., & Arnone, R. A. (2002). Deriving inherent optical properties from water color: a multiband quasi-analytical algorithm for optically deep waters. *Applied optics*, *41*(27), 5755-5772. https://doi.org/10.1364/AO.41.005755.

Lee, Z., Carder, K. L., Hawes, S. K., Steward, R. G., Peacock, T. G., & Davis, C. O. (1994). Model for the interpretation of hyperspectral remote-sensing reflectance. *Applied Optics*, *33*(24), 5721-5732. https://doi.org/10.1364/AO.33.005721.

Lee, Z., Carder, K. L., Mobley, C. D., Steward, R. G., & Patch, J. S. (1998). Hyperspectral remote sensing for shallow waters. I. A semianalytical model. *Applied optics*, *37*(27), 6329-6338. https://doi.org/10.1364/AO.37.006329.

Lee, Z., Carder, K. L., Mobley, C. D., Steward, R. G., & Patch, J. S. (1999). Hyperspectral remote sensing for shallow waters: 2. Deriving bottom depths and water properties by optimization. *Applied optics*, *38*(18), 3831-3843. https://doi.org/10.1364/AO.38.003831.

Lee, Z., Hu, C., Shang, S., Du, K., Lewis, M., Arnone, R., & Brewin, R. (2013). Penetration of UV-visible solar radiation in the global oceans: Insights from ocean color remote sensing. *Journal of Geophysical Research: Oceans*, *118*(9), 4241-4255. https://doi.org/10.1002/jgrc.20308.

Lee, Z., Shang, S., Du, K., & Wei, J. (2018). Resolving the long‐standing puzzles about the observed Secchi depth relationships. *Limnology and Oceanography*. https://doi.org/10.1002/lno.10940.

Lee, Z., Shang, S., Hu, C., Du, K., Weidemann, A., Hou, W., & Lin, G. (2015a). Secchi disk depth: A new theory and mechanistic model for underwater visibility. *Remote sensing of environment*, *169*, 139-149. https://doi.org/10.1016/j.rse.2015.08.002.

Lee, Z., Wei, J., Voss, K., Lewis, M., Bricaud, A., & Huot, Y. (2015b). Hyperspectral absorption coefficient of "pure" seawater in the range of 350–550 nm inverted from remote sensing reflectance. *Applied Optics*, *54*(3), 546-558. https://doi.org/10.1364/AO.54.000546.

Maritorena, S., Morel, A., & Gentili, B. (1994). Diffuse reflectance of oceanic shallow waters: Influence of water depth and bottom albedo. *Limnology and oceanography*, *39*(7), 1689-1703. https://doi.org/10.4319/lo.1994.39.7.1689.

Matsushita, B., Yang, W., Yu, G., Oyama, Y., Yoshimura, K., & Fukushima, T. (2015). A hybrid algorithm for estimating the chlorophyll-a concentration across different trophic states in Asian inland waters. *ISPRS journal of photogrammetry and remote sensing*, *102*, 28-37. https://doi.org/10.1016/j.isprsjprs.2014.12.022.

Mishra, S., Mishra, D. R., & Lee, Z. (2014). Bio-optical inversion in highly turbid and cyanobacteria-dominated waters. *IEEE Transactions on Geoscience and Remote Sensing*, *52*(1), 375-388. https://doi.org/10.1109/TGRS.2013.2240462.

Mitchell, B. G., Kahru, M., Wieland, J., Stramska, M., & Mueller, J. L. (2002). Determination of spectral absorption coefficients of particles, dissolved material and phytoplankton for discrete water samples. *Ocean optics protocols for satellite ocean color sensor validation, Revision*, *3*(2), 231.

Mobley, C. D. (1999). Estimation of the remote-sensing reflectance from above-surface measurements. *Applied optics*, *38*(36), 7442-7455. https://doi.org/10.1364/AO.38.007442.

Moore, T. S., Dowell, M. D., Bradt, S., & Verdu, A. R. (2014). An optical water type framework for selecting and blending retrievals from bio-optical algorithms in lakes and coastal waters. *Remote sensing of environment*, *143*, 97-111. https://doi.org/10.1016/j.rse.2013.11.021.

Morel, A. (1974). Optical properties of pure water and pure sea water. *Optical aspects of oceanography*, *1*, 22.

National Institute for Environmental Studies (2016) Lake Kasumigaura Database, National Institute for Environmental Studies, Japan. Accessed via http://db.cger.nies.go.jp/gem/moni-e/inter/GEMS/database/kasumi/index.html on 29-05-2018.

Olmanson, L. G., Bauer, M. E., & Brezonik, P. L. (2008). A 20-year Landsat water clarity census of Minnesota's 10,000 lakes. *Remote Sensing of Environment*, 112(11), 4086-4097. https://doi.org/10.1016/j.rse.2007.12.013.

Olmanson, L. G., Brezonik, P. L., Finlay, J. C., & Bauer, M. E. (2016). Comparison of Landsat 8 and Landsat 7 for regional measurements of CDOM and water clarity in lakes. *Remote Sensing of Environment*, 185, 119-128. https://doi.org/10.1016/j.rse.2016.01.007.

Philpot, W. D. (1989). Bathymetric mapping with passive multispectral imagery. *Applied optics*, *28*(8), 1569-1578. https://doi.org/10.1364/AO.28.001569.

Pope, R. M., & Fry, E. S. (1997). Absorption spectrum (380–700 nm) of pure water. II. Integrating cavity measurements. *Applied optics*, *36*(33), 8710-8723. https://doi.org/10.1364/AO.36.008710.

Preisendorfer, R. W. (1986). Secchi disk science: Visual optics of natural waters. *Limnology and* *oceanography*, *31*(5), 909-926. https://doi.org/10.4319/lo.1986.31.5.0909.

Rodrigues, T., Alcântara, E., Watanabe, F., & Imai, N. (2017). Retrieval of Secchi disk depth from a reservoir using a semi-analytical scheme. Remote Sensing of Environment, 198, 213-228. https://doi.org/10.1016/j.rse.2017.06.018.

Ruddick, K. G., Ovidio, F., & Rijkeboer, M. (2000). Atmospheric correction of SeaWiFS imagery for turbid coastal and inland waters. *Applied optics*, *39*(6), 897-912. https://doi.org/10.1364/AO.39.000897.

Secchi, P. A. (1864). Relazione delle esperienze fatte a bordo della pontificia pirocorvetta Imacolata Concezione per determinare la trasparenza del mare. *Memoria del PA Secchi. Il Nuovo Cimento Giornale de Fisica, Chimica e Storia Naturale, Ottobre 1864*, Published 1865, 20, 205-237.

Spyrakos, E., O'Donnell, R., Hunter, P. D., Miller, C., Scott, M., Simis, S. G., ... & Bresciani, M. (2018). Optical types of inland and coastal waters. *Limnology and Oceanography*, *63*(2), 846-870. https://doi.org/10.1002/lno.10674.

Shang, S., Lee, Z., Shi, L., Lin, G., Wei, G., & Li, X. (2016). Changes in water clarity of the Bohai Sea: Observations from MODIS. *Remote Sensing of Environment*, 186, 22-31.

Tyler, J. E. (1968). The secchi disc. *Limnology and oceanography*, 13(1), 1-6. https://doi.org/10.4319/lo.1968.13.1.0001.

Verschuur, G. L. (1997). Transparency measurements in Garner Lake, Tennessee: The relationship between Secchi depth and solar altitude and a suggestion for normalization of Secchi depth data. *Lake and Reservoir Management*, 13(2), 142-153. https://doi.org/10.1080/07438149709354305.

Wang, M., & Shi, W. (2007). The NIR-SWIR combined atmospheric correction approach for MODIS ocean color data processing. *Optics Express*, *15*(24), 15722-15733. https://doi.org/10.1364/OE.15.015722.

Wang, Y., Shen, F., Sokoletsky, L., & Sun, X. (2017). Validation and Calibration of QAA Algorithm for CDOM Absorption Retrieval in the Changjiang (Yangtze) Estuarine and Coastal Waters. *Remote Sensing*, *9*(11), 1192. https://doi.org/10.3390/rs9111192.

Watanabe, F., Mishra, D. R., Astuti, I., Rodrigues, T., Alcântara, E., Imai, N. N., & Barbosa, C. (2016). Parametrization and calibration of a quasi-analytical algorithm for tropical eutrophic waters. *ISPRS Journal of Photogrammetry and Remote Sensing*, 121, 28-47. https://doi.org/10.1016/j.isprsjprs.2016.08.009.

Wei, J., Lee, Z., & Shang, S. (2016). A system to measure the data quality of spectral remote‐sensing reflectance of aquatic environments. *Journal of Geophysical Research: Oceans*, 121(11), 8189-8207. https://doi.org/10.1002/2016JC012126.

Wernand, M. R. (2010). On the history of the Secchi disc. *Journal of the European Optical*

Society-Rapid publications, 5. https://doi.org/10.2971/jeos.2010.10013s.

Yang, W., Matsushita, B., Chen, J., Yoshimura, K., & Fukushima, T. (2013). Retrieval of inherent optical properties for turbid inland waters from remote-sensing reflectance. *IEEE Transactions on Geoscience and Remote Sensing*, *51*(6), 3761-3773. https://doi.org/10.1109/TGRS.2012.2220147.

Yang, W., Matsushita, B., Chen, J., Yoshimura, K., & Fukushima, T. (2014). Application of a semianalytical algorithm to remotely estimate diffuse attenuation coefficient in turbid inland waters. *IEEE Geoscience and Remote Sensing Letters*, *11*(6), 1046-1050. https://doi.org/10.1109/LGRS.2013.2284343.

Yang, W., Matsushita, B., Yoshimura, K., Chen, J., & Fukushima, T. (2015). A Modified Semianalytical Algorithm for Remotely Estimating Euphotic Zone Depth in Turbid Inland Waters. *IEEE Journal of Selected Topics in Applied Earth Observations and Remote Sensing*, *8*(4), 1545-1554. https://doi.org/10.1109/JSTARS.2015.2415853.

Yarger H.L. & McCauley J.R. (1975) Quantitative water quality with Landsat and Skylab. In Proc., *NASA Earth Resources Survey Symposium, Houston*, pp.347–369.

Zhang, X., Hu, L., & He, M. X. (2009). Scattering by pure seawater: effect of salinity. *Optics Express*, *17*(7), 5698-5710. https://doi.org/10.1364/OE.17.005698.

Zhao, D., Cai, Y., Jiang, H., Xu, D., Zhang, W., & An, S. (2011). Estimation of water clarity in

Taihu Lake and surrounding rivers using Landsat imagery. Advances in Water Resources, 34(2), 165-173. https://doi.org/10.1016/j.advwatres.2010.08.010.